AMERICAN SOCIETY of
GENE & CELL
THERAPY

Characterization and Molecular Mechanism of Peptide-Conjugated Gold Nanoparticle Inhibiting p53-HDM2 Interaction in Retinoblastoma

Sushma Kalmodia,[1,2] Sowmya Parameswaran,[3] Kalaivani Ganapathy,[1] Wenrong Yang,[2] Colin J. Barrow,[2] Jagat R. Kanwar,[4] Kislay Roy,[4] Madavan Vasudevan,[5] Kirti Kulkarni,[5] Sailaja V. Elchuri,[1] and Subramanian Krishnakumar[1]

[1]Department of Nano Biotechnology, Vision Research Foundation, Sankara Nethralaya, 18, College Road, Nungambakkam, Chennai 600 006, India; [2]Centre for Chemistry and Biotechnology, Deakin University, Geelong Campus, Waurn Ponds, VIC 3216, Australia; [3]Radheshyam Kanoi Stem Cell Laboratory, Vision Research Foundation, Sankara Nethralaya, 18, College Road, Nungambakkam, Chennai 600 006, India; [4]Nanomedicine –Laboratory of Immunology and Molecular Biomedical Research (NLIMBR), School of Medicine (SoM), Centre for Molecular and Medicine Research (C-MMR), Deakin University, Geelong Campus, Waurn Ponds, VIC 3217, Australia; [5]Bionivid Technologies, Bangalore 560043, India

Inhibition of the interaction between p53 and HDM2 is an effective therapeutic strategy in cancers that harbor a wild-type p53 protein such as retinoblastoma (RB). Nanoparticle-based delivery of therapeutic molecules has been shown to be advantageous in localized delivery, including to the eye, by overcoming ocular barriers. In this study, we utilized biocompatible gold nanoparticles (GNPs) to deliver anti-HDM2 peptide to RB cells. Characterization studies suggested that GNP-HDM2 was stable in biologically relevant solvents and had optimal cellular internalization capability, the primary requirement of any therapeutic molecule. GNP-HDM2 treatment in RB cells *in vitro* suggested that they function by arresting RB cells at the G2M phase of the cell cycle and initiating apoptosis. Analysis of molecular changes in GNP-HDM2-treated cells by qRT-PCR and western blotting revealed that the p53 protein was upregulated; however, transactivation of its downstream targets was minimal, except for the PUMA-BCl2 and Bax axis. Global gene expression and *in silico* bioinformatic analysis of GNP-HDM2-treated cells suggested that upregulation of p53 might presumptively mediate apoptosis through the induction of p53-inducible miRNAs.

INTRODUCTION

Retinoblastoma (RB), which is caused by mutations in the RB1 tumor suppressor gene, is the most common pediatric eye cancer. The two main aims of treating RB are to prevent the spread of the disease, or metastasis, and to preserve vision. Enucleation is the main treatment modality in advanced stages of the disease, when the tumor occupies important regions of the visual field and is limited to one eye.[1,2] Chemotherapy is preferred when a germline mutation is identified that predisposes the patient to develop secondary cancers.[3–6] However, some patients present with tumors that do not occupy the major visual fields, and, in these patients, localized targeted therapies are possible. Recently, several studies have focused on either activating tumor suppressors or suppressing other oncogenes to aid in the treatment of RB.[7–9]

An oncogene that is highly expressed in most cancers, with some evidence in RB tumors, is human double minute 2 (HDM2).[10–13] Under normal conditions, cellular homeostasis is established by way of a feedback loop involving HDM2 and p53. However, during tumorigenesis, the feedback loop is lost, either due to the amplification of HDM2 or due to mutations in p53. Inhibition of the HDM2 protein or blocking its interaction with p53 would be useful when HDM2 is overexpressed, but not when a wild-type p53 is absent.[14] In almost all RB tumors, a wild-type p53 protein is present; however, it is rendered non-functional because of the interaction of HDM2, leading to its ubiquitination and eventually to its degradation.[15,16] Therefore, targeting HDM2 in RB is a potential therapeutic strategy.[17–19]

Previous studies employing small molecules and HDM2 peptides have revealed that blocking p53 and HDM2 interaction leads to reduced cell proliferation and increased apoptosis in RB cells.[10,20,21]

Earlier, a transducible peptide incorporating the TAT sequence was used for the delivery of anti-HDM2 peptide.[10] Although the study revealed a significant functional effect, the presence of the positively charged amino acids arginine and lysine in the TAT peptide (YGRKKRRQRRR) make them vulnerable to cleavage by proteolytic enzymes, which might necessitate repeated administration of the peptides.[22] Therefore, stability of the peptide needs to be considered for sustainable and effective therapeutic response. In particular, with respect to ocular delivery, several physiological and anatomical barriers exist that restrict the dispersion and bioavailability of drugs including peptides. Therefore, use of non-invasive approaches such

as microneedles, transscleral diffusion, and iontophoresis, coupled with nanoparticle-based drug conjugates, might be advantageous for overcoming ocular barriers and also for increasing the efficiency and availability of the drugs delivered intraocularly.[23–26]

Gold nanoparticles (GNPs) have been advocated for therapeutic agent delivery owing to their large surface-area-to-volume ratio, which enables adsorption of several hundred molecules on its surface. However, studies have shown that synthetic chemicals used in the synthesis of GNPs are not suitable for many biological applications owing to their toxicity. We have earlier reported a rapid method for the synthesis of GNPs using the extracts of *Vitis vinefera L*. GNPs thus synthesized were found to be non-toxic and biocompatible to normal retinal glial cells.[27] In this study, we utilize biocompatible GNP-synthesized *Vitis vinefera L.* to deliver HDM2 peptide and establish the therapeutic potential of GNP-HDM2 in RB through functional knockdown of HDM2 protein. In addition, we provide insight on the molecular mechanisms that may be engaged during the functional HDM2 knockdown by GNP-HDM2 treatment of RB, by global gene expression analysis.

Our results indicate that GNP-HDM2 is functional and affects the survival of RB by inhibiting cell proliferation by arresting cells at the G2M phase and accentuating the apoptotic program through the PUMA-BCL2-BAX axis. Additionally, global gene expression analysis indicated that mitotic cell phase, ubiquitin-mediated proteoloysis, endocytosis and p53-mediated tumor suppressor microRNAs (miRNAs), are involved in the functional effects observed. The current study establishes the functional effect of GNP-HDM2 on RB, using a Y79 cell line model and investigating the possible molecular mechanistic network orchestrating the therapeutic response.

RESULTS

HDM2 Expression Analysis in RB Tumors

The data on HDM2 overexpression in RB tumors from different studies are inconsistent.[13,28,29] Hence, we attempted to study HDM2 expression in a clinically well-defined cohort (Tables S1A and S1B) by gene and protein expression, to rationalize its potential for targeted therapy in RB. The gene expression analysis of RB tumors revealed that *HDM2* was significantly overexpressed in RB cells compared to normal cells (Figures 1A and 1B). Nine out of 10 RB tumors analyzed showed a greater than 2-fold increase in the *HDM2* gene expression compared to normal retina. Since functioning of *HDM2* requires the HDM2 protein to be translated, we analyzed the expression of HDM2 protein in the RB tumors. In line with the gene expression, the protein expression analysis revealed overexpression of HDM2 in all the five samples analyzed compared to normal retina (Figures 1C–1E).

In Vitro Characterization and Functional Study of GNP-HDM2

GNPs were conjugated to different molar concentrations of the HDM2 peptide at a ratio of 1:1, 1:2, and 1:3 (GNP:HDM2), and the shift in the absorption maxima (λmax) was analyzed using UV-visible (UV-vis) spectrophotometery (Figure S1). There was no significant

difference in the λmax between GNP 1:1 and 1:2, whereas 1:3 showed a visible difference in λmax peak intensity that did not change significantly with increasing peptide concentration. Hence, 1:3 was considered the ratio of saturation and chosen for further experimentation.

Surface plasmon resonance (SPR-λ_{SPR}) of GNP-HDM2 at 535–540 nm showed a significant increase in the absorbance at 1:3 (Figure S1A). The presence of free HDM2 peptide could directly interfere with the functioning of GNP-HDM2, therefore the conjugate was subjected to ultracentrifugation ($\sim$30,000 rpm for 20−30 min). Spectroscopic analysis at the absorption maxima of 220 nm (λmax for free peptide) of the supernatants revealed no specific peak, indicating absence of free peptide in the conjugates prepared (data not shown). A red shift from $\sim$532 nm indicates loading of the peptide onto the GNP (Figure 2A), owing to the increase in absorbance at the λmax (Figure S1A). In addition to UV-vis spectroscopic analysis, the GNP and GNP-HDM2 were characterized by dynamic light scattering (DLS), Fourier-transform infrared spectroscopy (FTIR), X-ray photoelectron spectroscopy (XPS), and transmission electron microscopy (TEM) analysis.

DLS Analysis of GNP-HDM2

The hydrodynamic diameters (HD) and polydispersity index (PDI) of GNP-HDM2, GNP:Scb, and GNP were measured using DLS. The observed HD was 66.72 ± 2.83 with a PDI of 0.303 and 50.40 ± 2.190 with a PDI 0.37 for GNP:HDM2 and GNP:Scb, respectively. The GNP revealed a HD of 24.47 ± 0.028 with a PDI of 0.388. The size distribution of GNP-HDM2 (Figure 2B), GNP (Figure 2C), and GNP-Scb (Figure S1B) were 32–122, 8–19, and 18–80 nm, respectively. An increase in HD of GNP-HDM2 and GNP-Scb compared to GNP indicates the presence of peptide on the surface of GNP. The presence of non-polar amino acid such as L in HDM2 peptide and V, P, and L in the Scb peptide allows for a π-π interaction between the peptide and the GNP, which might explain the larger HD in GNP-HDM2 and GNP-Scb.[30]

Similarly, the zeta potential (ζ) was obtained −11.4, −18.2, and −16.7 mV for GNP-HDM2, GNP, and GNP-Scb (Figures S1C–S1E). Overall, the change in the HD, size distribution and zeta potential was in accordance with the SPR shift observed in case of GNP-HDM2 and GNP-Scb compared to GNP. The auto correlation g1 (τ) curve (Figures S2A–S2C) confirms monomodal distribution, and confirmed GNP, GNP:Scb, and GNP:HDM2 were monodispered and spherical.

FTIR Analysis of GNP-HDM2

FTIR was performed to identify the functional groups present in the GNP-HDM2 and GNP-Scb conjugate. The major functional groups present in the conjugate and in HDM2 and Scb peptides are listed in Table S2A (Figures S3A and S3B). The FTIR spectra of GNP-HDM2 and GNP-Scb showed broad spectral features at 3,918, 3,410, and 3,402 cm^{-1}, which are attributed to the N-H stretching vibration in GNP-HDM2 and GNP-Scb. The band at 2,146 cm^{-1} shifted to 2,134 cm^{-1} for GNP-HDM2, because of the Au-S bond

GENE EXPRESSION OF HDM2

PROTEIN EXPRESSION OF HDM2
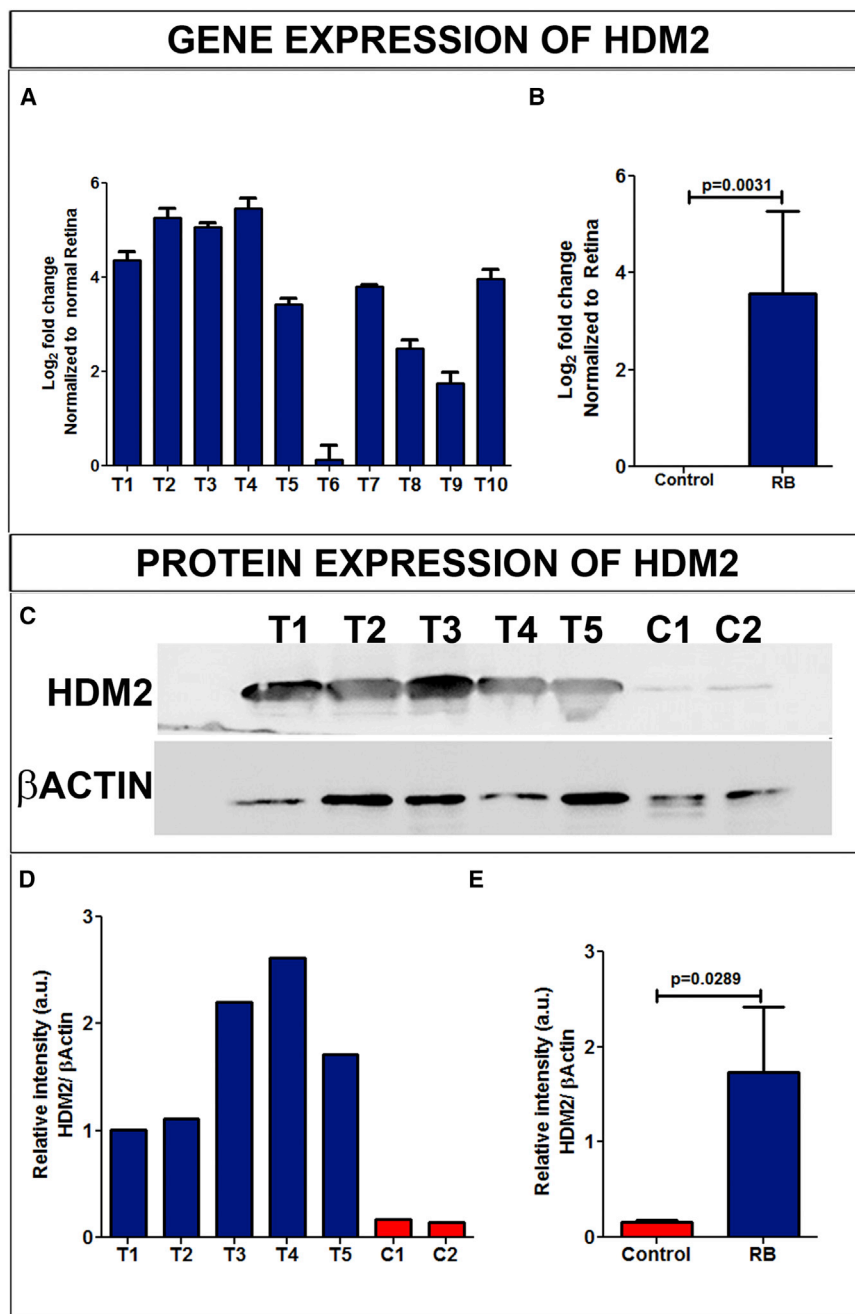
Figure 1. Expression of HDM2 in Retinoblastoma Tumors

(A) qRT-PCR revealed a greater than 2-fold ($\log_2$ = 1) increase in 9 out of 10 RB tumor samples. log2 values were calculated using the delta-delta Ct method with β-actin as the endogenous control and normal cadaveric retina as the calibrator. (B) The expression of HDM2 transcripts was significantly upregulated in retinoblastoma compared to the control (normal cadaveric retina) (p = 0.0031; two-tailed t test). (C) Western blotting of HDM2 and β-actin revealed increased HDM2 protein expression in RB (n = 5) compared to the control (normal cadaveric retina; n = 2). Lanes: T1–T5: RB tumors, C1, C2: control (normal cadaveric retina). (D) The relative intensity of HDM2 protein normalized to endogenous β-actin levels was higher in RB compared to the control. (E) Expression of HDM2 protein in RB was significantly upregulated compared to the control (p = 0.0289; two-tailed t test).

scb peptide (1,649 cm^{-1}), respectively, which was attributed to the involvement of peptide bonding with GNP. In addition, 508–496 cm^{-1} exclusively observed in the fingerprint region of GNP-HDM2 also supported bond formation between the GNPs and the HDM2 peptide.
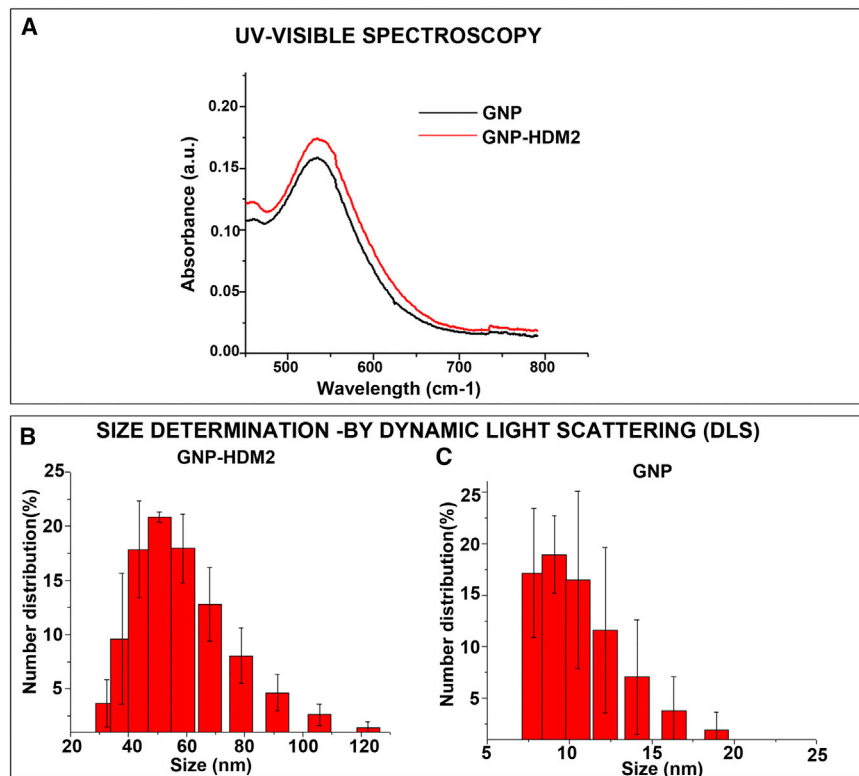
XPS Analysis of GNP-HDM2

XPS analysis was carried out on GNP and GNP-HDM2 to establish the nature of the chemical bonds in the particles. A wide XPS scan showed the spectra of the major peak C1s, O1s, and N1s and higher resolution spectra for the Au4f and S2p in GNP and GNP-HDM2 (Figures 3A–3F). In the high-resolution spectra of the Au4f region of GNP, two different peaks were observed at 83.44 and 87.00 eV (Figures 3A–3C), and similar peaks were observed for GNP-HDM2 at 84.30 and 87.30 eV, corresponding to Au4f7/2 and Au4 f 5/2 for Au^0 and $Au\ 1^+$, respectively (Figures 3D–3F). Neutral atoms or small-sized particles of gold show the Au^0 state. It is assumed that disulphide of the MPA linker of HDM2 peptide leads to oxidation of the GNPs, which changes Au (0) to Au (1) in the GNP-HDM2-conjugated state for Au4f7/2.[33,34] The peak of 84.30 eV for Au4f7/2 suggests the presence of an Au-S bond in GNP-HDM2.[35,36] However, the higher binding energy at 87.00 and 87.30 eV corresponds to a Au^{3+} oxidative state of the Au. For the S2p region, the peak at 164.75 in GNP represents sulfur (S-S) species, which indicates that proteins are present in the reducing agent (*Vitis vinifera L.*) of GNP. The presence of high binding energy S2p peaks at 167–168 eV indicates the presence of

from the mercaptopropionic acid linker to the peptide. A similar shift was observed in GNP-Scb from 2,137 cm^{-1} to 2,145 cm^{-1}. In addition to these peaks, additional peaks were observed in the range 1,041–1,053 cm^{-1} and 798–644 cm^{-1}, which indicates the presence of sulfur functional groups in the peptide.[31,32]

There was a shift toward higher frequency with respect to the carbonyl amide vibration in GNP-HDM2 (1,654 cm^{-1}) and GNP-Scb (1,656 cm^{-1}) compared to HDM2 (1,650 cm^{-1}) and

A

UV-VISIBLE SPECTROSCOPY

B

SIZE DETERMINATION -BY DYNAMIC LIGHT SCATTERING (DLS)

Figure 2. UV-Visible Spectroscopy and Dynamic Light Scattering Characterization of GNP-HDM2

(A) UV-visible spectroscopy of GNP-HDM2 and the GNP was carried out. A shift of ∼5 nm was observed in the surface plasmon resonance (SPR) peak in GNP-HDM2 (red line) with respect to the GNP (black line). (B and C) Dynamic light scattering (DLS) data show the size of nanoparticles (% number distribution) in GNP-HDM2 (B) and the GNPs (C). See also Figures S1, S2, and S5.

sulfones (S-O), affirming the oxidation of the S2p peak. This confirms the self-assembly of HDM2 peptide on GNP.[37–39] Taken together, the XPS analysis confirmed the conjugation of the HDM2 peptide with the GNPs in the GNP-HDM2 conjugate as revealed by oxidation of Au4f 7/2 and S2p.[40]
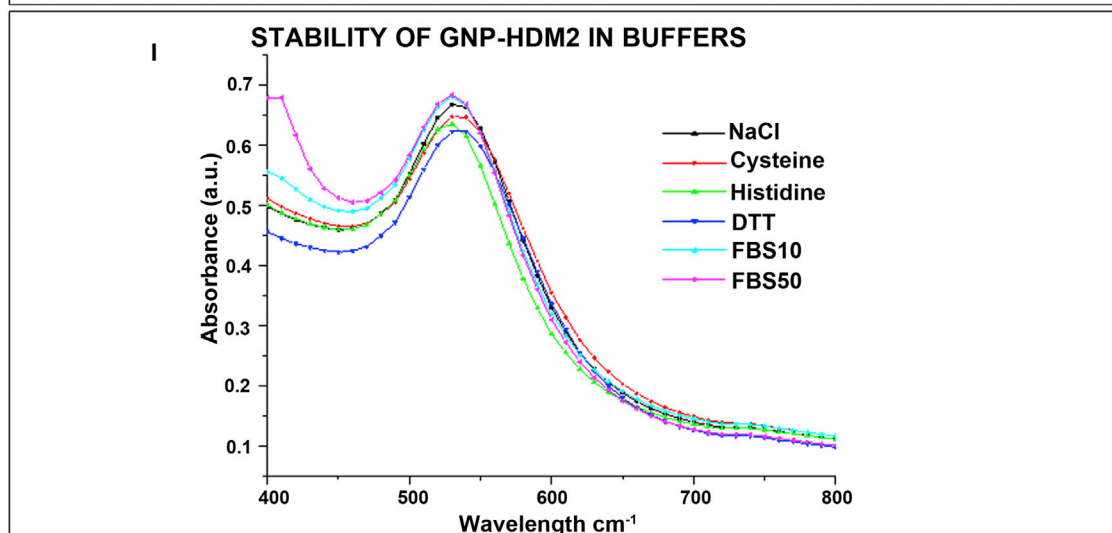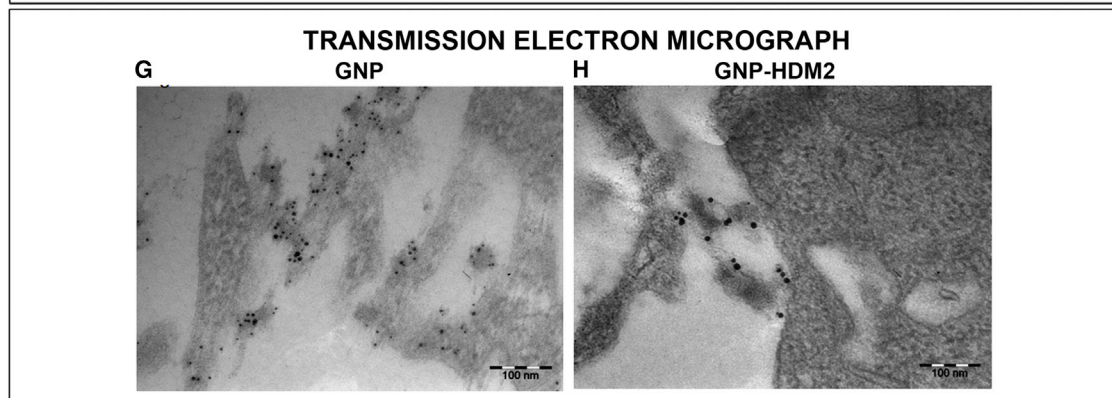
TEM Analysis of GNP-HDM2

TEM was used to determine the shape and the size of both the GNP and the GNP-HDM2 peptide. Both GNP and GNP-HDM2 were spherical in shape and were approximately 12–15 nm in size (Figures 3G and 3H). TEM also revealed internalization of the particles inside the cells and the absence of particle aggregation, a prerequisite for a stable system.

MALDI-TOF Analysis of GNP-HDM2 and In Silico Molecular Dynamics Studies

MALDI-TOF analysis of the GNP and GNP-HDM2 confirmed the binding of HDM2 peptide with the GNPs. The molecular weight of HDM2 peptide is 1,565.70. In the MALDI-TOF analysis, the most intense peak was observed at 1,553.39 m/z with several multiplet near the peak (Figures S4A and S4B). We hypothesized that there is a possibility of some rearrangement which could lead to the change in the mass of peptide after binding to the GNPs. To understand this difference, we predicted the structure of the peptides by simulation using GROMACS (v.4.5) suite.[41,42] The *in silico* data confirmed that the peptide is linear in structure (Figures S4C and S4D). However, the presence of aromatic rings of the amino acids

(Phe [F] and Trp [W]) in the HDM2 peptide showed greater fluctuations,[43] which in turn was reflected as a shift in the m/z value (1,553.39 instead of 1,565.70) of the most intense peak of the peptide on the GNP. The other common peaks (m/z) between the GNP and GNP-HDM2 correspond to major compounds present in reducing agent (*Vitis vinifera* extract) used in GNP preparation (Table S2B).[44]

Hyperspectral Imaging of GNP-HDM2

Hyperspectral imaging of GNP-HDM2 was carried out to understand the distribution of GNP-HDM2 and GNP in cells 24 hr post-treatment (Figures S4E and S4F). The results suggest that the particles are uniformly distributed in both the groups suggesting the stability of the GNP-HDM2 conjugate.[45]

Buffer and Ionic Strength of GNP-HDM2

The ionic stability of GNP-HDM2 was studied in different solvents to confirm its long-term use as a therapeutic biomolecule.[46] The ionic strength of GNP-HDM2 was confirmed by studying the SPR size and potential using different solvents that are relevant to cellular application. The SPR (λ_{SPR}) position for different solvents is shown in Figure 3I. The λmax was ∼535–537 nm with no considerable shift (either red or blue) in SPR peak position in all solvents tested, confirming the stability and lack of change in the optical properties of GNP-HDM2. In the presence of the polar amino acids histidine and cysteine, the zeta potential was −25.6 ± 1.59 mV and −19.7 ± 2.30 mV, respectively, indicating bond formation between polar amino acids and GNP-HDM2. Similarly, DTT also increased the negative zeta potential from −11.4 to −48.1 ± 0.5 mV. The increased negative potential in the presence of DTT (−48.1 ± 0.5 mV) and amino acid confirmed the stability of GNP-HDM2 in polar solvents and strong reducing agents, respectively. Similarly, a change in zeta potential was reported in nitrogen doped carbon with DTT functionalized.[47] As reported, anionic DTT increased the negative potential, whereas in the presence of NaCl, a high ionic strength salt, the zeta potential did not alter as much as in the other solvents and amino acids. NaCl maintained the electric double layer on GNP-HDM2 and did not alter the ionic stability of GNP-HDM2.[48,49] In contrast, fetal bovine serum (FBS) significantly decreased the negative zeta potential −7.80 ± 0.77 mV, which could be

X-RAY PHOTOELECTRON SPECTROSCOPY

A

Intensity (CPS) vs Binding energy(ev)

Au4f, S2p, C1s, N1s, O1s

B GNP

Intensity (CPS) vs Binding energy (ev)

Au4f7/2, Au4f5/2

- Original spectra
- Au4f-1
- Au4f-2
- Au4f-fitted spectra

C

Intensity (CPS) vs Binding energy (ev)

- Original spectra
- Fitted spectra

D

Intensity (CPS) vs Binding energy(ev)

Au4f, S2p, C1s, N1s, O1s

E GNP-HDM2

Intensity (CPS) vs Binding energy (ev)

- Original spectra
- Au4f-1
- Au4f-2
- Fitted Au4f-1
- Fitted Au4f-2
- Fitted spectra

F

Intensity (CPS) vs Binding energy (ev)

TRANSMISSION ELECTRON MICROGRAPH

G GNP

100 nm

H GNP-HDM2

100 nm

STABILITY OF GNP-HDM2 IN BUFFERS

I

Absorbance (a.u.) vs Wavelength cm^{-1}

- NaCl
- Cysteine
- Histidine
- DTT
- FBS10
- FBS50

(legend on next page)

Table 1. Ionic and Solvent Stability of GNP-HDM2

S. No.	Solvent	Z Average[a]	Zeta Potential (mV)
1	GNP-HDM2 +NaCl	54.79 ± 0.81	−13.6 ± 0.87[b]
2	GNP-HDM2 +cysteine	53.51 ± 0.26	−19.7 ± 2.30[b]
3	GNP-HDM2 +histidine	41.64 ± 0.28	−25.6 ± 1.59[b]
4	GNP-HDM2 +DTT	44.57 ± 0.18	−48.1 ± 0.5[b]
5	GNP-HDM2 +10% FBS	57.14 ± 3.23	−8.26 ± 0.2[c]
6	GNP HDM2 +50% FBS	23.40 ± 0.56	−7.80 ± 0.77[c]
7	GNP-HDM2	66.72 ± 2.83	−11.43 ± 0.55

The change in zeta potential toward more negative (−13.6 ± 0.87 mV to 48.1 ± 0.5 mV) compared with GNP-HDM2 (−11.43 ± 0.55 mV) confirmed the stability of GNP-HDM2 in highly ionic solvents and buffers.
[a]Z average indicates the intensity-based mean hydrodynamic size of GNP-HDM2 subjected to the solvent type.
[b]Indicates electric bilayer of different solvents on GNP-HDM2. The zeta potential increased toward more negative.
[c]Indicates the FBS coating on GNP-HDM2 that changed the zeta potential toward less negative. This finding confirms the binding of the FBS protein to GNP-HDM2.

due to binding or coating of FBS proteins on GNP-HDM2 (Table 1). Overall, the change in zeta potential and its magnitude indicated the colloidal stability of GNP-HDM2 in various biologically relevant solutions, making these acceptable for their biological applications.[50]

Functional Effect of GNP-HDM2 and GNP on Y79 Cell Lines

Our earlier study on non-cancerous retinal glial (MIOM1) cells identified a concentration of 50 μM GNP to be non-toxic at the end of a 24-hr treatment. Hence that concentration was used to prepare GNP-HDM2. Y79 cells were treated with 50 μM GNP and GNP-HDM2 for 24 hr and the cells were analyzed for apoptosis and cell proliferation by Annexin V-PI and PI-Ribonuclease staining, respectively. The fraction of cells in G0/G1; S; G2M phases were analyzed to reveal the effect of GNP and GNP-HDM2 on the cell-cycle analysis. The results did not reveal any major difference between the different cell phases between the groups, however, a statistically significant decrease in the cells in G1 phase (p = 0.0217; one-way ANOVA) with concomitant increase in the G2M phase (p = 0.0142; one-way ANOVA) in GNP-HDM2-treated cells compared to control, suggesting that GNP-HDM2 might function by arresting cells at the G2/M phase (Figures 4A–4D). However, the difference was not significant between the GNP- and GNP-HDM2-treated cells.

The analysis of the Y79 cells treated with GNP and GNP-HDM2 for apoptosis revealed that there was a significant increase in the cells

undergoing apoptosis in the GNP-HDM2-treated group compared to both the control and GNP treated cells (p = 0.0010; one-way ANOVA and Tukey's test for multiple group comparisons) (Figures 4E–4H).

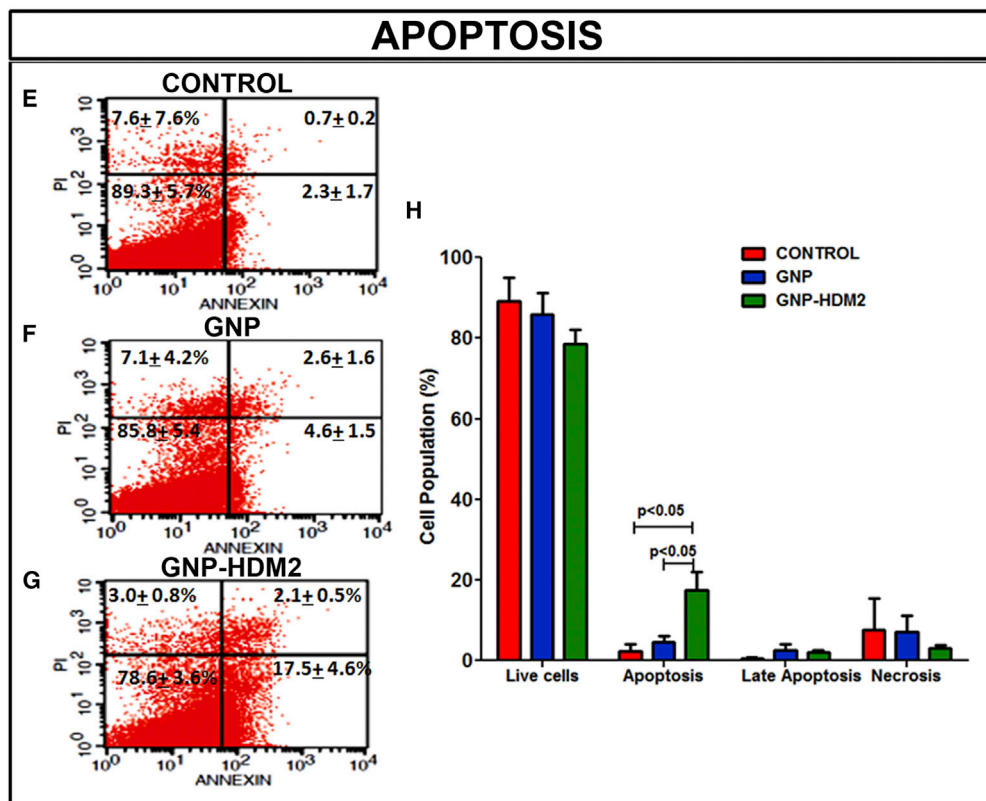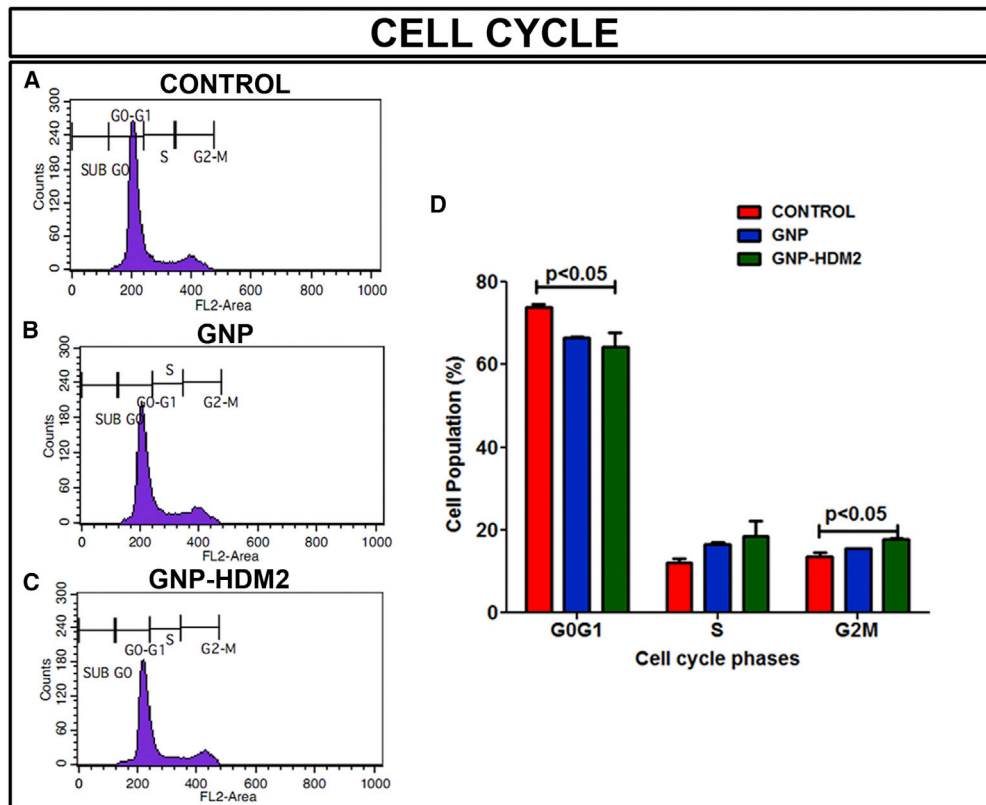### Analysis of p53 and Its Downstream Targets in the GNP-HDM2 and GNP Treatments

Since, the HDM2 peptide primarily functions by increasing the stability of p53 protein.[10] We evaluated the transcript levels of *p53* in GNP, GNP-Scrambled peptide (GNP-Scr), and GNP-HDM2 groups, compared to the untreated control. There was a significant increase in the transcript levels of *p53* in GNP-HDM2 and GNP compared to the GNP-Scr group and untreated control (p = 0.0015, one-way ANOVA) (Figure 5A). The *P53* level was downregulated in GNP-Scr compared to the untreated control. Hence, GNP was preferred over GNP-Scr for further comparative analysis.

We further evaluated the levels of p53 protein in the control, GNP and GNP-HDM2 groups and found that similar to transcript levels, p53 protein was significantly increased in both GNP and GNP-HDM2 groups compared to control (p < 0.0001; one-way ANOVA) (Figures 5B and 5C). However, the levels remained comparable between GNP and GNP-HDM2, which made in depth evaluation of GNP and GNP-HDM2 groups more important.

Since, p53 transcriptionally activate HDM2,[51] we studied its expression at the gene and protein levels. HDM2 transcripts and protein were found to be significantly downregulated in the GNP-HDM2 group compared to both control and GNP at p < 0.0001, p = 0.0004, respectively (Figures 5D and 5E). Since, this result was unforeseen and encouraging, we screened for other direct p53 transcriptional targets[52–54] and related molecules, to know if the p53 arm was activated. qPCR analysis of *p21^{cip1}*, *PUMA*, *BAX*, *BCL2* and *CASP3*(Caspase 3) revealed that the increase in the p53 protein levels did not upregulate *p21^{cip1}* in either treatment. With respect to the p53-dependent apoptotic pathway molecules, *PUMA* was upregulated in the GNP-HDM2 group compared to both control and GNP-treated cells (Figure 5F). The levels of *BCL2*, an indirect target of p53, and *BAX*, a direct target of p53,[54–56] were both downregulated compared to the control (Figure 5F). The ratio of *BAX:BCL2* was significantly increased in the GNP-HDM2 group compared to both control and GNP-treated groups, indicating p53-PUMA-BCL2 and BAX axis molecules were involved in the apoptosis of GNP-HDM2-treated RB cells (Figure 5F). The decrease in *p21^{cip1}* did not

Figure 3. X-Ray Photoelectron Spectroscopy and Transmission Electron Microscopy of GNP-HDM2
(A–F) A wide XPS scan showed the spectra of the major peak C1s, O1s, and N1s (A) and higher-resolution spectra for Au4f and S2p (B) and the original and fitted spectra in the GNPs. In the high-resolution spectra of the Au4f region of the GNPs, two different peaks were observed at 83.44 and 87.00 eV. A wide XPS scan showed the spectra of the major peaks C1s, O1s, and N1s (D); higher resolution spectra for Au4f and S2p (E); and the original fitted spectra (F) in the GNP-HDM2. Peaks were observed for GNP-HDM2 at 84.30 and 87.30 eV, corresponding to Au4f7/2 and Au4f5/2 for Au[0] and Au 1[+], respectively. (G and H) Transmission electron microscopy (TEM) revealed that both GNP-HDM2 (G) and the GNPs (H) are ∼12–15 nm in size, with a spherical shape. (I) The stability of GNP-HDM2 in different solvents showed that SPR (λmax) remained between 535–537 nm without any considerable shifts (either red or blue) in all the solvents, confirming a stable optical property in these solvents. Scale bar, 100 nm (G and H). See also Figures S3 and S4.

CELL CYCLE

A CONTROL

B GNP

C GNP-HDM2

D

- CONTROL
- GNP
- GNP-HDM2

p<0.05

p<0.05

APOPTOSIS

E CONTROL

7.6±7.6%   0.7±0.2

89.3±5.7%   2.3±1.7

F GNP

7.1±4.2%   2.6±1.6

85.8±5.4   4.6±1.5

G GNP-HDM2

3.0±0.8%   2.1±0.5%

78.6±3.6%   17.5±4.6%

H

- CONTROL
- GNP
- GNP-HDM2

p<0.05

p<0.05

(legend on next page)

come as a surprise, since its involvement pertains more to the G1-S phase transition and the cell-cycle analysis data of the treatments showed cell-cycle arrest at the G2M phase, without significantly affecting the G1-S phase transition. Overall, the activation of p53 by GNP-HDM2 led to increased apoptosis via activation of PUMA and the BCL2-BAX axis.

Analysis of Global Gene Expression Effects in GNP-HDM2- and GNP-Treated RB Cells

To gain further insight into the mechanistic network involved in GNP-HDM2-treated cells, microarray was performed on the control, GNP- and GNP-HDM2-treated Y79 cells (GEO: GSE92987). Differential gene expression analysis between the control and the GNP-treated group revealed that the molecular profile between the two groups did not vary greatly, with only 68 genes being differentially expressed. Of these 68 genes, 65 were upregulated and 3 were downregulated (Figure 6A). Gene ontology (GO) and Kyoto Encyclopedia of Genes and Genomes (KEGG) pathway analysis did not reveal any statically significant enrichment between the control and GNP-treated groups, suggesting that the specific dose of GNP did not significantly alter the molecular profiling of the cells. To compare the differential gene expression between GNP- and GNP-HDM2-treated cells, gene expression was compared between two groups, namely GNP versus control and GNP-HDM2 versus control. The fold change for the genes between GNP versus control (Figures 6A and 6C) and GNP-HDM2 versus control (Figures 6B and 6D) were utilized to calculate the fold difference between the GNP and GNP-HDM2 groups. The analysis revealed that 815 genes were upregulated and 812 were downregulated in GNP-HDM2 cells, relative to GNP-treated cells (Figure 6E).

To determine the significant biological functions and pathways involved during GNP-HDM2 treatment, functional analysis by GO, KEGG pathway, and ingenuity pathway analysis was performed. GO revealed 194 and 213 terms significantly enriched in downregulated and upregulated gene lists, respectively. The five most overrepresented GO terms for biological functions in the downregulated and upregulated genes are provided in Table S3.

The biological function predominantly enriched in the downregulated genes pertained to the mitotic phase of the cell cycle correlating with the G2M arrest of the cell-cycle analysis. However, the biological function analysis on the upregulated genes were broad and pertained

to several physiological functions such as cellular differentiation, immune response, organ development, indicating that the genes that are upregulated predominantly orchestrate the conversion of undifferentiated cells such as tumor into a more differentiated cells that might have functional implications. The cellular component ontology clearly differentiated the downregulated and upregulated gene lists, as the former was predominantly intracellular, including cytoplasmic, cytoskeletal, and nuclear components, and the latter was enriched exclusively with extracellular and membrane-bound proteins (Table S4). Independent analysis using the human protein reference database confirmed the GO results (Figure 6F). The molecular function ontology revealed predominance of enzymatic functions and receptor activity in downregulated and upregulated gene sets, respectively (Table S5).

The pathways enriched in the downregulated and upregulated gene list by KEGG pathway analysis are provided in Table S6. The most enriched pathways in the downregulated set of genes included cellular processes like the cell cycle, ubiquitin-mediated proteolysis, and endocytosis. Comprehensive analysis of the genes participating in ubiquitin-mediated proteolysis revealed that GNP-HDM2 treatment not only leads to a reduction in HDM2 but also to a reduction in other E3 ubiquitin ligases such as COP1 and PIRH2, which can individually target p53 leading to its degradation.[57,58] This suggests that there is a concerted action on the prevention of other ubiquitin ligases from degrading p53, leading to increased stability of the p53 protein in the treated cells. In addition to the downregulation of ubiquitin ligases, the downregulation of the gene CDC23, which is required for mitosis and G1 phase of the cell cycle, suggests that the concerted inhibition of both the cell cycle and ubiquitin-mediated proteolysis may be attributed to the G2M arrest and increased P53 stability and apoptosis that were observed in the functional experiments.

In addition to the cell cycle and ubiquitin-mediated proteolysis, a significant enrichment was seen in endocytosis in the downregulated gene lists. Most of the downregulated genes suggest that clathrin-dependent endocytosis is significantly compromised without much involvement of clathrin-independent endocytosis. Previous studies on breast cancer show that inhibition of clathrin-dependent endocytosis led to restoration of the death receptors on the cell surface, thereby sensitizing TRAIL-resistant cells to apoptosis. Several studies have linked ubiquitination with endocytosis with subsequent degradation of plasma membrane receptors and transporters. It is

Figure 4. Functional Effects of GNP and GNP-HDM2 on RB Cell Lines

(A–D) RB cells treated with the GNPs and GNP-HDM2 for 24 hr were subjected to cell-cycle analysis. Control (untreated) (A), GNP-treated (B), and GNP-HDM2-treated (C) cells were subjected to cell-cycle analysis by Telford's method. (D) Cell-cycle analysis revealed a statistically significant decrease in the number of cells in the G1 phase (p = 0.0217; one-way ANOVA) with a concomitant increase in the G2M phase (p = 0.0142; one-way ANOVA) in the number of GNP-HDM2-treated cells compared to the control, suggesting that the bioconjugate might function by arresting the cells at the G2/M phase. Error bar represents the mean ± SD of the triplicate samples. (E–H) RB cells treated with GNP and GNP-HDM2 for 24 hr were subjected to an apoptosis assay. Control (untreated) (E), GNP-treated (F), and GNP-HDM2-treated (G) cells were subjected to an apoptosis assay by the annexin V FITC-PI method. (H) An apoptosis assay revealed a significant increase in the number of cells undergoing apoptosis in the GNP-HDM2-treated group compared to both the control and GNP-treated cells (p = 0.0010; one-way ANOVA and Tukey's test for multiple group comparisons). Error bars represent the mean ± SD of triplicate samples. Lower left: live cells (annexin$^-$ and PI$^-$). Lower right: early apoptotic (annexin$^+$ and PI$^-$). Upper right: late apoptotic (annexin$^+$ and PI$^+$). Upper left: necrotic cells (annexin$^-$ and PI$^+$).
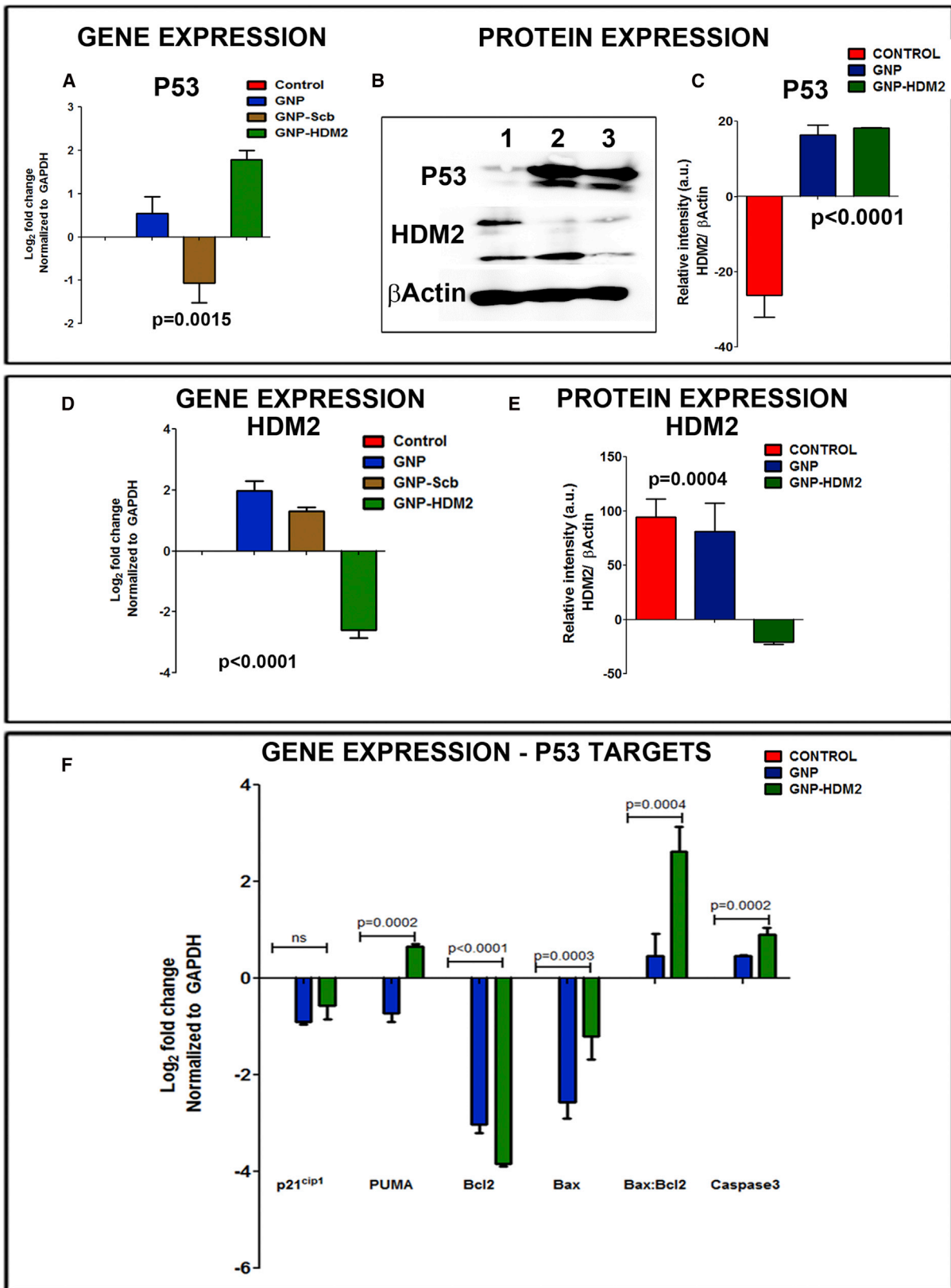
(legend on next page)

hypothesized that inhibition of E3 ubiquitin ligases, as discussed above, contributed to inhibition of the endocytosis process at the global level. Several studies have shown the efficacy of clathrin-mediated endocytosis inhibitors and dynamin endocytosis inhibitors in inhibiting tumorigenesis.

In the upregulated set of genes, the most enriched processes involve metabolism and signal transductions, such as arachidonic acid metabolism, calcium signaling, cytokine-cytokine interactions and olfactory transduction. With respect to arachidonic acid metabolism in tumorigenesis, several studies indicate a pro-tumorigenic role. However, with respect to RB, one study revealed that arachidonic acid increases oxidative stress in Y79-RB1 cells and promoted its apoptosis. It was shown that activation of PLA2 by the drug melittin led to apoptosis of RB cells. In the arachidonic acid pathway, upregulation of three different PLA2s, namely PLA2 group IIA, PLA2 group IIC, and PLA2 group IID, suggested that they influence the apoptotic mechanism in these cells. With respect to olfactory transduction, reports suggest that olfactory receptors are widely expressed in tissues other than sensory neurons of the olfactory epithelium, however, their functional relevance in these tissues have not been established. In the context of tumorigenesis, there are contradictory reports on the activation of olfactory receptors and promotion or inhibition of tumors. The role of calcium signaling and cytokine-cytokine receptor interactions in the tumorigenesis is not clear and requires further evaluation.

To gain insight into common regulators of the global gene expression post-HDM2 functional knockdown, upstream regulator analysis was carried out in Ingenuity pathway analysis. Upstream regulator analysis revealed eleven significant master regulator genes governing the gene expression networks (Fisher's exact test, $p < 0.05$). The 11 upstream regulators, their activation/ inhibition status and the class to which they belong are shown in Table S7. Of the 11 regulators, 8 showed activation, and 3 showed inhibition. The role of these upstream regulators in cancer is compiled in Table S7. Based on their roles in cancer, eight out of the eleven upstream regulators had tumor suppressor or anti-tumorigenic properties, while three had tumorigenic or tumor invasive properties. In addition to their roles in cancer, their relation to the p53-HDM2 axis revealed that 8 out of 11 regulators played important roles in modulating the p53-HDM2 axis or p53-directed downstream processes.

Detailed analysis revealed that p53-dependent activation of tumor suppressor miRNAs miR16-5p, let-7, mitochondrial protein, and interactive chromatin modifier SMARCB1 potentiate tumor suppression and apoptosis (Table S7). Concordantly, inhibition of the axis activating HDM2, namely ESR1 and RABL6, may also contribute to tumor suppression (Table S7). In contrast, the direct targets of p53, namely *NUPR1* and *TCF3*, might enhance tumorigenesis and chemoresistance, inadvertently increasing metastasis of the tumor (Table S7).

Since, the upstream regulator indicated p53-dependent miRNA activation plays a role in tumor suppression, we utilized an *in silico* approach to identify miRNA that were highly enriched in the dataset. For this purpose, we obtained a list of validated miRNA known to regulate the transcripts that are upregulated and downregulated post HDM2-GNP treatment. The miRNA were ranked based on the number of targets they regulated in a given list. The top 5 miRNA in each group are shown in Table S8. Since, the miRNA is known to inhibit mRNA expression, the miRNA list was consolidated based on the following criteria: (1) the miRNA that regulate the genes in the upregulated transcript list were considered as downregulated and (2) the miRNA that regulate the genes in the downregulated transcript list were considered as upregulated. The *in silico* analysis suggested that p53 regulated miRNAs, hsa-miR-192-5p, and hsa-miR-215-5p showed upregulation along with hsa-miR 16-5p, whereas hsa-miR-335-5p showed downregulation. The results suggest that HDM2-GNP might in part orchesterate miRNA-based tumor suppression via p53.

DISCUSSION

Herein we report the preparation, characterization and functional efficacy of GNP-HDM2 in RB. Our results indicate that GNP-HDM2 can reactivate wild-type p53 whose expression is compromised in RB tumors. Characterization of GNP-HDM2 revealed several advantages in utilizing it for intraocular treatment of RB. Assessment of the zeta-potential of GNP-HDM2 confirmed its stability in biologically relevant solutions. In addition, results of the cellular internalization by TEM and hyperspectral imaging, alongside its functional attributes on the cell cycle and apoptosis results suggested that the conjugate increased the stability of the peptide by protecting it against protease degradation, thereby increasing its delivery into the cytosol.

It has been observed that zeta potential showed a decrease in negative potential with -11.4 mV in GNP-HDM2 and -18.2 mV in the GNP, which might enhance internalization of the peptide.[59–61] A similar retention of overall negative charge has been reported, without compromising the biological function of the peptides or proteins. These studies showed that the overall negative potential of the GNP-peptide conjugates can be attributed to incomplete

Figure 5. Analysis of p53 and Its Downstream Targets in the GNP- and GNP-HDM2-Treated RB Cells

(A) Analysis of P53 by quantitative real-time PCR showed a significant increase in the P53 transcript levels in GNP-HDM2 and the GNPs over GNP-Scb and the untreated control (p = 0.0015; one-way ANOVA). (B) Representative western blot of p53 and HDM2 proteins in the control (untreated), GNP-, and GNP-HDM2-treated RB cells. (C) Analysis of p53 protein in both GNP- and GNP-HDM2-treated RB cells revealed an increase in p53 protein after both treatments. (D and E) Analysis of the HDM2 transcripts (D) and protein (E) revealed that, while the HDM2 gene and protein expression increased in GNP-treated cells, the cells treated with GNP-HDM2 showed a significant decrease in HDM2 expression. (F) qRT-PCR analysis of possible downstream targets of p53 revealed that the PUMA-BCl2-Bax axis led to caspase-mediated apoptosis; however, p21 expression was not significantly affected.
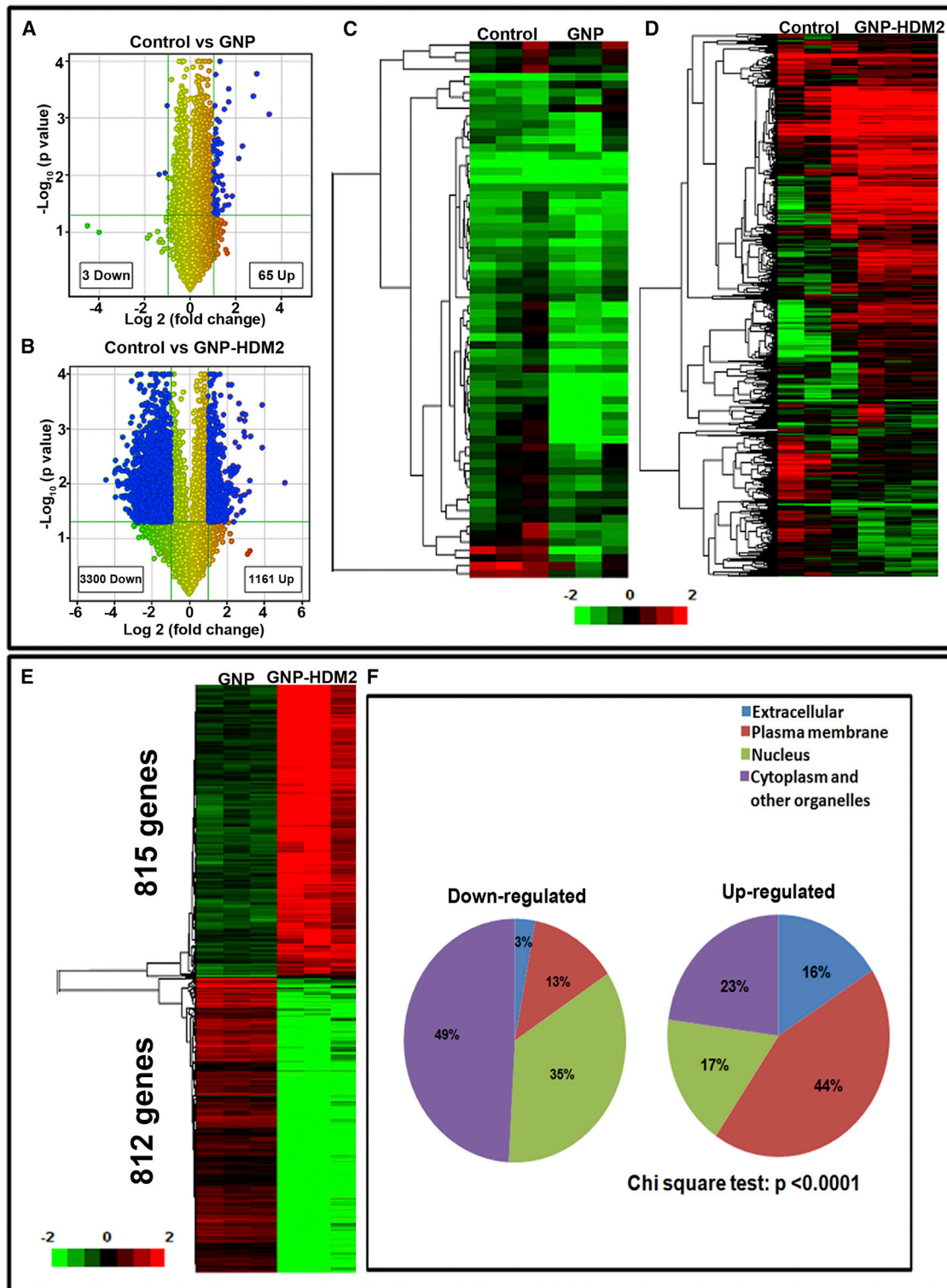
Figure 6. Global Gene Expression Analysis of GNP-HDM2 Treatment on Retinoblastoma Cells

(A) A volcano plot revealed 68 differentially expressed genes with 65 upregulated and 3 downregulated in GNP-treated cells compared to the control at a fold change of ≥ 2 and p value < 0.05. (B) A volcano plot revealed 4,461 differentially expressed genes with 1,161 upregulated and 3,300 downregulated in GNP-HDM2-treated cells compared
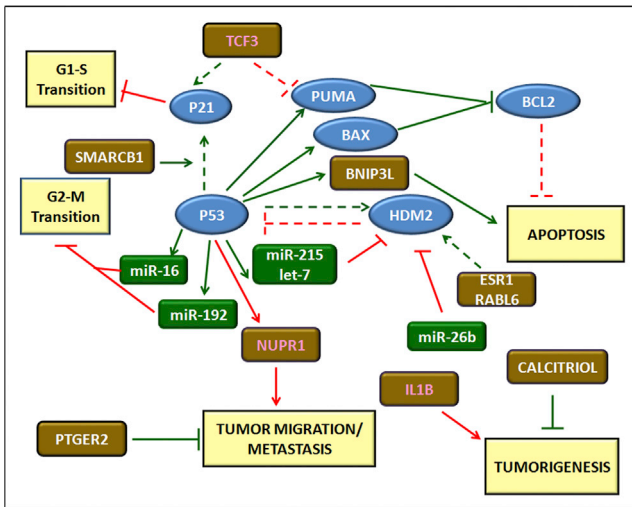
Figure 7. Schematic Representation of Presumptive Molecular Mechanism Orchestrated by GNP-HDM2 Treatment in Retinoblastoma

Predominant downstream targets of p53, upstream regulators, and miRNA identified by IPA analysis and *in silico* miRNA analysis are presented. Arrows indicate activation; straight line with bars indicate inhibition; dotted lines in arrow/bar indicate abrogation of the expected effect; green boxes reveal miRNA identified by *in silico* analysis; light-brown boxes reveal the molecules identified as upstream regulators by IPA analysis; light-blue ovals are validated by qPCR and/or western blotting; white and pink fonts indicate favorable and unfavorable molecules for tumor suppression, respectively; and yellow boxes indicate a functional outcome.

neutralization of the positive charge of the BBN peptide and TNF factors which were conjugated to the GNP.[36,62]

Our results on GNP-HDM2 treatment in an RB1 cell line confirmed that the nano-bio-conjugate interfered with the ubiquitin-mediated proteolysis of p53, thereby upregulating the p53 protein. Similar results of stable upregulation of p53 expression was recognized in previous studies employing peptides or small molecules against HDM2.[63–65] However, while the previous studies reported an increased transactivation of a wide range of downstream targets of the p53 protein, including increased expression of HDM2 transcript itself, GNP-HDM2 reduced the HDM2 transcript and the protein levels.

In addition, global gene expression analysis provided evidence of global suppression of E3 ubiquitin ligases that mediate p53 degradation. These data suggest that p53 expression was stabilized by suppression of ubiquitin-mediated proteolysis. Although a previous study utilizing the anti-HDM2 peptide suggested that both p21^{cip1}-

mediated G1-S phase arrest and p53-mediated apoptosis were involved in the outcome, instead GNP-HDM2 predominantly orchestrated its functional effect by arresting the cells at the G2-M phase p53-mediated apoptosis. A study reporting the effect of nutlin 3, a small molecule against HDM2 suggested that cellular response to nutlin 3 was context specific. Its treatment on cancer cell lines led to either cycle arrest or apoptosis, and this event was dependent on the RB expression and its phosphorylation.[46] The absence of RB1 expression in RB might have led to preferential apoptosis over G1-S cell-cycle arrest. Previous genetic screen for identification of pathway-specific regulators of p53 activation in different cell lines suggested that TCF3/E2A expression determine the p21:PUMA ratio upon p53 activation. The study suggested that depletion of TCF3 led to an impairment of cell-cycle arrest, while promoting p53 activation. However, in our study, the upstream regulator analysis suggested an activation of TCF3 with reversal of the p21:PUMA ratio. We hypothesize that factors other than TCF3, such as TRIAP1, which inhibits p21^{cip1}, might be involved in reversal of this role.[66] Our results with the upstream regulator analysis showed a strong correlation of p53-mediated miRNA activation.

The *in silico* analysis of miRNA using target enrichment analysis showed good concordance with the upstream regulator analysis. A study involving nutlin 3a treatment on multiple myeloma showed that the small molecule based p53 activation in these cells led to activation of miRNAs such as miR 192 and miR 215, which suppressed HDM2 expression. This finding corroborates our observation where stabilized p53 instead of transactivating HDM2 led to their suppression, indicating the p53-directed miRNA-mediated suppression of HDM2. Rigorous functional validation of p53-induced miRNA is required to confirm this finding. The overall molecular mechanism occurring during functional HDM2 knockdown by GNP-HDM2 treatment of RB is summarized as a schematic in Figure 7. In summary, the results indicate that GNP-HDM2 is effective in suppressing RB primarily by p53-mediated apoptosis. At this point, the *in silico* analysis indicates that miRNAs may be involved in orchestrating this effect, although we have not validated this experimentally. We consider the functional validation of these miRNA will serve as an ideal follow-up study for confirming the mechanism involved.

MATERIALS AND METHODS
Ethics Approval
The proposed study was approved by the ethics committee of Vision Research Foundation-Chennai, India, under the approval number 383-2013-P.

to the control at a fold change of ≥ 2 and p value < 0.05. (C and D) Unsupervised hierarchial clustering of differentially expressed genes in the control versus GNP (C) and the control versus GNP-HDM2 (D) groups. (E) Unsupervised hierarchial clustering of differentially expressed genes between the GNPs and GNP-HDM2. To compare the differential gene expression between GNP- and GNP-HDM2-treated cells, gene expression between two groups, namely GNPs versus control and GNP-HDM2 versus control were compared. The fold change for the genes between GNPs versus control and GNP-HDM2 versus control were utilized to calculate the fold difference between the GNP and GNP-HDM2 groups. The analysis revealed that 815 genes were upregulated and 812 were downregulated in GNP-HDM2-treated cells relative to GNP-treated cells. (F) The cellular component ontology by the human protein reference database clearly differentiated the downregulated and upregulated genes as the former was predominantly intracellular including cytoplasmic, cytoskeletal, and nuclear components, and the latter was exclusively enriched with extracellular and membrane-bound proteins.

Analysis of HDM2 Expression in RB Tissues

The HDM2 transcript and protein levels in RB tissues (n = 10) were analyzed in comparison to normal retina. Briefly, RB tumor samples were collected from the RB patients who underwent enucleation as part of their therapy at the Medical Research Foundation, Sankara Nethralaya (Chennai, India). Informed consent for utilizing the samples for research purposes was obtained from patients during the surgical procedure. The clinicopathological details of the patients included in the study are provided in Tables S1A and S1B. The RB tumor samples were snap frozen at −80°C and stored until use. The samples were thawed on ice and subjected to RNA and protein extraction. Cadaveric normal donor retina tissue was obtained from the CU Shah Eye Bank, Sankara Nethralaya (India). Total RNA was isolated from 100 mg of tissue using Trizol reagent (Sigma, USA). cDNA was synthesized from total RNA using the High-Capacity cDNA Reverse Transcription Kit (Applied Biosystems, USA). Quantitative real-time PCR was performed using the SYBR Green Mix (Applied Biosystem, USA) using HDM2 primers. The $\log_2$-fold change was calculated using the $\Delta\Delta CT$ method with GAPDH as an endogenous control, normalized to the control (cadaveric retina). For protein expression, approximately 250 mg of tissue was subjected to homogenization using a radio immunoprecipitation (RIPA) buffer and subjected to sonication with 10 cycles of 10-s pulses under ice-cold conditions. Protein was estimated using the Bradford's method. Western blotting was performed with 50 μg of protein separated on 10%–12% SDS-PAGE using HDM2 and β-actin antibody. Detailed protocols for qPCR and western blotting are provided in the Supplemental Materials and Methods.

Preparation of GNP-HDM2

HDM2 peptide (QETFSDLWKLLP, 12 amino acids) and a control peptide (KRLRLDPV, 8 amino acids) named "Scrambled" was custom synthesized by Sigma-Aldrich (Japan) (OE-14045-001 and OE-14045-002, respectively) with >95% high-performance liquid chromatography (HPLC) purged (Table S9). A 3-mercaptopropionic acid linker was attached to the N-terminal of HDM2 and the Scb peptide, and the observed mass of the peptides was 1,565.7 and 1,085.4 m/z, respectively. Figure S5 shows the schematic representation of the conjugation of GNPs with the HDM2 peptide. GNP-HDM2 and GNPs-Scb were prepared by mixing functionalized HDM2 and Scb peptide with GNP, synthesized using *Vitis vinefeara L.*[26] GNP-HDM2 was prepared by mixing GNPs with peptide: 18 mL of GNPs (optical density 520 [OD$_{520}$] = 1.00 nm) (242×10^{-6}, mol gold/L) with 4.2 mg of peptide (GNP:HDM2 1:3) (dissolve in 0.01 cell-culture-grade DMSO), with continuous stirring for 24 hr followed by purification using ultra-centrifugation at 30,000 rpm until a clear supernatant was obtained and any unbound peptide was removed. A similar protocol was followed for the 1:2 and 1:1 GNP:HDM2 by mixing 2.8 and 1.40 mg of peptide, respectively. The absence of unbound peptide was confirmed by UV-vis spectroscopy at 220 nm. The pellet was resuspended in the cell culture medium, and OD was measured at 530 nm to get the final concentration of GNP-HDM2 and GNPs-Scb, using GNP as a standard followed by their characterization. A final stock concentration of 50 μg/mL was prepared for the further experimentation.

Characterization of Synthesized GNP-HDM2

UV-vis Spectroscopy

GNP-HDM2 and GNP:Scb were characterized by UV-vis spectroscopy, and spectral data were collected in the 400- to 800-nm range at room temperature. A 1-cm light path quartz cuvette was used, and samples were diluted and OD adjusted (OD$_{520}$ = 1.00 nm).

DLS

The average hydrodynamic size (Z average), size distribution (% number distribution), and zeta potential were determined, with 3 measurements being collected for each sample using DLS (Zetasizer [Nano-ZS model equipped with 4.0 mW, 633 nm laser, Model ZEN3600, serial no. MAL1024433, Malvern Instruments, Malvern, UK]).

Fourier Transform Infrared Spectrum

HDM2 and Scb peptides and conjugate GNP:HDM2 and GNP:Scb were characterized by FTIR (Vortex 70, BRUKER). FTIR was performed over the range 500–4,000 cm^{-1}, in transmittance mode using potassium bromide (KBr) pellets.

XPS

XPS was performed to determine the chemical bonding states between the GNPs and the peptide at the surface region. XPS analysis was performed at the Indian Institute of Science (Banglore, India). An XPS spectrometer with an Al Kα energy source at 1,486.6 eV, anode source operated at 250 W, and pressure below 2×10^{-9} torr was used for the scans. Samples were prepared by drop-coating of the GNP:HDM2-conjugated solution on a clean silicon wafer, and the drops were allowed to air dry. The electron pass energy was set at 0–1,000 eV for wide/survey scans and 180 eV for high-resolution scans of Au4f and S2p. All XPS spectra were calibrated by calibrating the charge against the hydrocarbon C1s peak at 284.6 eV as a reference.

TEM for Cellular Internalization and Characterization

The particle shape and size were further confirmed by TEM. The GNPs and GNP-HDM2 were prepared by drop-coating on copper grids and dried overnight. TEM analysis was carried out at an accelerating voltage of 200 kV. For the TEM study, $\sim 1 \times 10^6$ Y79 cells were cultured in 6-well plates and treated with GNP and GNP-HDM2 for 24 hr. These cells were washed with PBS and fixed in a primary fixative (2.5% glutaraldehyde prepared using 0.1 M sodium cacodylate buffer at pH 7.2–7.4.). The detailed TEM analysis protocol is provided in the Supplemental Materials and Methods.

MALDI-TOF Analysis of GNP-HDM2 and *In Silico* Molecular Dynamic Studies

MALDI-TOF Analysis of the GNPs and GNP-HDM2

MALDI-TOF was performed using a cyano-4-hydroxycinnamic acid (HCCA) matrix for analysis of proteins and peptides. The solvent was 50% MeCN and 0.1% trifluoroacetic acid (TFA) in water at 1:1 ratio. The sample concentration was 10 – 100 pmol/μL. Equal volumes (1 μL) of HCCA matrix and sample were mixed, and 2 μL of the

mixture was spotted on a MALDI target plate and allowed to dry to perform the MALDI-TOF analysis using Bruker RapiFleX at Shrimpex Multidisciplinary Biotech (Chennai, India).

In silico molecular dynamics of the peptide were performed using GROMACS. The AMBER force field was employed to calculate the interactions of simulation. The peptide was solvated in a cubic box of TIP3P H_2O, and the charge of the system was neutralized by adding either chloride or sodium ions. The neutralized system was minimized and then equilibrated with NPT-NVT ensembles. The production run was initially carried out for 10 ns and extended up to 50 ns depending on the convergence of the system. The structure for the peptide sequence was modeled by performing homology modeling with PDB (PDB: 1YCR) structure as a template. Further, the model was refined using molecular dynamics simulations. A root-mean-square deviation (RMSD) plot was used to assess the stability of the model.

Hyperspectral Imaging of GNP-HDM2

Y79 cells cultured in RPMI media on coverslips (Lab-Tek) overnight were treated with the 50 μM of GNPs and GNP-HDM2 for 24 hours. Post-incubation, the cells were washed with 1× PBS and fixed in 4% paraformaldehyde solution. Permanent slides were prepared using mountant and imaged using the Hyperspectral Imaging System (Cytoviva) at IITM (India).

In Vitro Ionic and Buffer Stability

GNP-HDM2 was studied in a variety of solvents and buffers to affirm its stability *in vitro* for the functional studies, using previously reported methodology. Briefly, 1 mL of GNP-HDM2 was mixed with 0.5 mL (10 mM) each of DTT, cysteine, histidine NaCl, and FBS. GNP alone (without HDM2 peptide) served as the control. The solutions were then incubated for 2 hr at room temperature, and the stability of GNP-HDM2 was determined by size and zeta potential measurement.

Functional Studies Using an *In Vitro* RB Model
Treatment of Y79 (RB) Cell Lines with GNP-HDM2

The Y79 cell line was obtained from Cell Bank, RIKEN Bio Resource Centre (Ibaraki, Japan) and cultured in suspension using RPMI 1640 (GIBCO, USA) cell culture media. The culture media was supplemented with FBS 10% (v/v) (GIBCO, USA) and 1% antibiotic cocktail (v/v). All experiments were performed within 5 passages of its retrieval.

Analysis of p53-HDM2 Axis in GNP-HDM2 in RB-Treated Cells

Real-time PCR and western blotting were performed to check the expression of HDM2 and P53 in the Y79 cells treated with GNP and GNP-HDM2 (described earlier in the Materials and Methods; the Supplemental Materials and Methods). For analyzing p53-dependent transactivation, real-time PCR for p53 targets such as Bax, PUMA, Bcl2, and p21 was performed using the method detailed in the Supplemental Materials and Methods. The primer sequence and antibody details are provided in the Supplemental Materials and Methods text, respectively (Table S10).

Functional Effect of GNP-HDM2 Treatment on RB Cell Viability and Cell Proliferation

The functional effect of GNP-HDM2 treatment on Y79 cell line was studied by cell-cycle analysis and an apoptosis assay. Briefly, Y79 cells were seeded at a density of 1×10^6 per well in a 6-well plate. The cultured cells were allowed to grow overnight and treated with 50 μM concentration of GNP-HDM2 and GNP (control) for 24 hr. For the cell-cycle analysis, cells were harvested post-treatment and washed in cold 1× PBS. After washing, cells were fixed in 1 mL cold 70% (v/v) ethanol for 30 min on ice. The fixed cells were washed twice in ice-cold 1× PBS. Subsequently, cells were incubated with Telford's reagent and incubated for 3 hr at 37°C and analyzed in a FACSCalibur Flow Cytometer. For the apoptosis assay, the cells post-treatment were washed with cold 1× PBS. The cells were diluted in 1× annexin buffer to achieve a density of 1×10^6 cells/mL. 5 μL of Alexa Fluor 488 annexin V in 100 μL of cell suspension was incubated for 15 min. Subsequently, 1 μL of PI (propidium iodide) was added, and samples were incubated for 5 min. After incubation, the cell suspension was mixed with 300 μL 1× annexin-binding buffer and was kept on ice. This was followed by analysis of the stained cells using flow cytometry, involving the measurement of fluorescence emission at 530 and 617 nm using a 488-nm excitation laser, with 10,000 events recorded for each sample. All experiments were performed in triplicate.

Microarray Investigation of Molecular Signaling during GNP-HDM2 and GNP Treatment

Global gene expression analysis was undertaken to investigate the regulation of exponentially growing Y79 cells, which were treated with 50 μM of GNP-HDM2 or GNP for 24 hr and used for microarray analysis. Briefly, the treated Y79 cells were processed for RNA isolation (RNeasy Mini Kit, QIAGEN, USA), followed by cDNA conversion, using a recommended protocol from Affymetrix (https://www. thermofisher.com/us/en/home/life-science/microarray-analysis.html). Genechip PrimeView Human Arrays were used for hybridization (Affymetrix, Santa Clara, CA, USA), and scanning and feature extraction was also done using GCOS software. The microarray data are available in GEO (GEO: GSE92987). CEL files were analyzed utilizing the R/Bioconductor package, one Channel GUI. Affymetrix whole-genome expression raw data were RMA16 and were normalization and preprocessed using GeneSpring GX (v.12.5) software (Agilent Technologies, Santa Clara, CA, USA). Differentially expressed probe tests (Genes) upon treatment in comparison to untreated cells were identified by considering statistically significantly enriched transcripts ($p \leq 0.05$). The functional classification of differentially expressed genes including the GO enrichment analysis and KEGG pathway was performed using the Database for Annotation, Visualization, and Integrated Discovery (DAVID) tool. The cellular localization of the differential gene expression was carried out by analyzing the list in the Human protein reference database (http://www.hprd.org/). The gene identifiers and corresponding expression and significance values were uploaded into ingenuity pathway analysis (IPA) software for the upstream regulator analysis. A Fisher's exact test p value and activation score (z) were calculated to assess the significance of enrichment of the gene expression data for the genes downstream of an upstream regulator.

In Silico MicroRNA Analysis

The gene-miRNA interactions for the differentially expressed genes were obtained from the validated target module of miRwalk (v.2.0) (http://zmf.umm.uni-heidelberg.de/apps/zmf/mirwalk2/genepub.html). Briefly, the list of gene identifiers that were upregulated or downregulated genes post-GNP-HDM2 were individually uploaded into the validated gene-miRNA interaction information retrieval system of miRwalk (v.2.0) (http://zmf.umm.uni-heidelberg.de/apps/zmf/mirwalk2/genepub.html). The list of miRNAs obtained was filtered to include those which target at least 50 genes and ranked based on the number of genes they affect. This approach was utilized for both the upregulated and downregulated transcript lists.

SUPPLEMENTAL INFORMATION

Supplemental Information includes Supplemental Materials and Methods, five figures, and ten tables and can be found with this article online at https://doi.org/10.1016/j.omtn.2017.10.012.

AUTHOR CONTRIBUTIONS

CONFLICTS OF INTEREST

Authors declare no conflict of interest.

ACKNOWLEDGMENTS

REFERENCES

1. Mendoza, P.R., and Grossniklaus, H.E. (2016). Therapeutic options for retinoblastoma. Cancer Contr. 23, 99–109.

2. Shields, C.L., and Shields, J.A. (2010). Retinoblastoma management: advances in enucleation, intravenous chemoreduction, and intra-arterial chemotherapy. Curr. Opin. Ophthalmol. 21, 203–212.

3. Shields, C.L., Fulco, E.M., Arias, J.D., Alarcon, C., Pellegrini, M., Rishi, P., Kaliki, S., Bianciotto, C.G., and Shields, J.A. (2013). Retinoblastoma frontiers with intravenous, intra-arterial, periocular, and intravitreal chemotherapy. Eye (Lond.) 27, 253–264.

4. Shields, C.L., Honavar, S.G., Meadows, A.T., Shields, J.A., Demirci, H., Singh, A., Friedman, D.L., and Naduvilath, T.J. (2002). Chemoreduction plus focal therapy for retinoblastoma: factors predictive of need for treatment with external beam radiotherapy or enucleation. Am. J. Ophthalmol. 133, 657–664.

5. De Potter, P. (2002). Current treatment of retinoblastoma. Curr. Opin. Ophthalmol. 13, 331–336.

6. Marr, B.P., Brodie, S.E., Dunkel, I.J., Gobin, Y.P., and Abramson, D.H. (2012). Three-drug intra-arterial chemotherapy using simultaneous carboplatin, topotecan and melphalan for intraocular retinoblastoma: preliminary results. Br. J. Ophthalmol. 96, 1300–1303.

7. Schwermer, M., Dreesmann, S., Eggert, A., Althoff, K., Steenpass, L., Schramm, A., Schulte, J.H., and Temming, P. (2017). Pharmaceutically inhibiting polo-like kinase 1 exerts a broad anti-tumour activity in retinoblastoma cell lines. Clin. Experiment. Ophthalmol. 45, 288–296.

8. Weng, Y., Liu, J., Jin, S., Guo, W., Liang, X., and Hu, Z. (2017). Nanotechnology-based strategies for treatment of ocular disease. Acta Pharm. Sin. B 7, 281–291.

9. Dyer, M.A. (2016). Lessons from retinoblastoma: implications for cancer, development, evolution, and regenerative medicine. Trends Mol. Med. 22, 863–876.

10. Harbour, J.W., Worley, L., Ma, D., and Cohen, M. (2002). Transducible peptide therapy for uveal melanoma and retinoblastoma. Arch. Ophthalmol. 120, 1341–1346.

11. Karni-Schmidt, O., Lokshin, M., and Prives, C. (2016). The roles of MDM2 and MDMX in cancer. Annu. Rev. Pathol. 11, 617–644.

12. Davitt, K., Babcock, B.D., Fenelus, M., Poon, C.K., Sarkar, A., Trivigno, V., Zolkind, P.A., Matthew, S.M., Grin'kina, N., Orynbayeva, Z., et al. (2014). The anti-cancer peptide, PNC-27, induces tumor cell necrosis of a poorly differentiated non-solid tissue human leukemia cell line that depends on expression of HDM-2 in the plasma membrane of these cells. Ann. Clin. Lab. Sci. 44, 241–248.

13. Ioachim, E., Charchanti, A., Stavropoulos, N.E., Skopelitou, A., Athanassiou, E.D., and Agnantis, N.J. (2000). Immunohistochemical expression of retinoblastoma gene product (Rb), p53 protein, MDM2, c-erbB-2, HLA-DR and proliferation indices in human urinary bladder carcinoma. Histol. Histopathol. 15, 721–727.

14. Prives, C., and White, E. (2008). Does control of mutant p53 by Mdm2 complicate cancer therapy? Genes Dev. 22, 1259–1264.

15. Nork, T.M., Poulsen, G.L., Millecchia, L.L., Jantz, R.G., and Nickells, R.W. (1997). p53 regulates apoptosis in human retinoblastoma. Arch. Ophthalmol. 115, 213–219.

16. Debbas, M., and White, E. (1993). Wild-type p53 mediates apoptosis by E1A, which is inhibited by E1B. Genes Dev. 7, 546–554.

17. Pritchard, E.M., Dyer, M.A., and Guy, R.K. (2016). Progress in Small Molecule Therapeutics for the Treatment of Retinoblastoma. Mini Rev. Med. Chem. 16, 430–454.

18. Zhang, B., Golding, B.T., and Hardcastle, I.R. (2015). Small-molecule MDM2-p53 inhibitors: recent advances. Future Med. Chem. 7, 631–645.

19. Elison, J.R., Cobrinik, D., Claros, N., Abramson, D.H., and Lee, T.C. (2006). Small molecule inhibition of HDM2 leads to p53-mediated cell death in retinoblastoma cells. Arch. Ophthalmol. 124, 1269–1275.

20. Carvajal, D., Tovar, C., Yang, H., Vu, B.T., Heimbrook, D.C., and Vassilev, L.T. (2005). Activation of p53 by MDM2 antagonists can protect proliferating cells from mitotic inhibitors. Cancer Res. 65, 1918–1924.

21. Vassilev, L.T. (2007). MDM2 inhibitors for cancer therapy. Trends Mol. Med. 13, 23–31.

22. Koren, E., Apte, A., Sawant, R.R., Grunwald, J., and Torchilin, V.P. (2011). Cell-penetrating TAT peptide in drug delivery systems: proteolytic stability requirements. Drug Deliv. 18, 377–384.

23. Shah, S.S., Denham, L.V., Elison, J.R., Bhattacharjee, P.S., Clement, C., Huq, T., and Hill, J.M. (2010). Drug delivery to the posterior segment of the eye for pharmacologic therapy. Expert Rev. Ophthalmol. 5, 75–93.

24. Lam, T.T., Edward, D.P., Zhu, X.A., and Tso, M.O. (1989). Transscleral iontophoresis of dexamethasone. Arch. Ophthalmol. 107, 1368–1371.

25. Patel, A., Patel, M., Yang, X., and Mitra, A.K. (2014). Recent advances in protein and peptide drug delivery: a special emphasis on polymeric nanoparticles. Protein Pept. Lett. 21, 1102–1120.

26. Gómez-Gaete, C., Fattal, E., Silva, L., Besnard, M., and Tsapis, N. (2008). Dexamethasone acetate encapsulation into Trojan particles. J. Control. Release *128*, 41–49.

27. Kalmodia, S., Harjwani, J., Rajeswari, R., Yang, W., Barrow, C.J., Ramaprabhu, S., Krishnakumar, S., and Elchuri, S.V. (2013). Synthesis and characterization of surface-enhanced Raman-scattered gold nanoparticles. Int. J. Nanomedicine *8*, 4327–4338.

28. Brennan, R.C., Federico, S., Bradley, C., Zhang, J., Flores-Otero, J., Wilson, M., Stewart, C., Zhu, F., Guy, K., and Dyer, M.A. (2011). Targeting the p53 pathway in retinoblastoma with subconjunctival Nutlin-3a. Cancer Res. *71*, 4205–4213.

29. Saxena, P., Kashyap, S., Bajaj, M.S., Pushker, N., Ghose, S., and Kaur, J. (2012). Expression of p53 and Mdm2 in human retinoblastoma. J. Clin. Exp. Ophthalmol. *3*, 236.

30. Wu, R.H., Nguyen, T.P., Marquart, G.W., Miesen, T.J., Mau, T., and Mackiewicz, M.R. (2014). A facile route to tailoring peptide-stabilized gold nanoparticles using glutathione as a synthon. Molecules *19*, 6754–6775.

31. Salaam, A.D., Hwang, P., McIntosh, R., Green, H.N., Jun, H.-W., and Dean, D. (2014). Nanodiamond-DGEA peptide conjugates for enhanced delivery of doxorubicin to prostate cancer. Beilstein J. Nanotechnol. *5*, 937–945.

32. Aryal, S., B K C, R., Dharmaraj, N., Bhattarai, N., Kim, C.H., and Kim, H.Y. (2006). Spectroscopic identification of S-Au interaction in cysteine capped gold nanoparticles. Spectrochim. Acta A Mol. Biomol. Spectrosc. *63*, 160–163.

33. Govindaraju, S., Ankireddy, S.R., Viswanath, B., Kim, J., and Yun, K. (2017). Fluorescent gold nanoclusters for selective detection of dopamine in cerebrospinal fluid. Sci. Rep. *7*, 40298.

34. Camci, M.T., Ulgut, B., Kocabas, C., and Suzer, S. (2017). In-situ XPS monitoring and characterization of electrochemically prepared Au nanoparticles in an ionic liquid. ACS Omega *2*, 478–486.

35. Tao, W., Ziemer, K.S., and Gill, H.S. (2014). Gold nanoparticle-M2e conjugate coformulated with CpG induces protective immunity against influenza A virus. Nanomedicine (Lond.) *9*, 237–251.

36. Chanda, N., Kattumuri, V., Shukla, R., Zambre, A., Katti, K., Upendran, A., Kulkarni, R.R., Kan, P., Fent, G.M., Casteel, S.W., et al. (2010). Bombesin functionalized gold nanoparticles show in vitro and in vivo cancer receptor specificity. Proc. Natl. Acad. Sci. USA *107*, 8760–8765.

37. Ulman, A., Ioffe, M., Patolsky, F., Haas, E., and Reuvenov, D. (2011). Highly active engineered-enzyme oriented monolayers: formation, characterization and sensing applications. J. Nanobiotechnology *9*, 26.

38. Tour, J.M., Jones, L., Pearson, D.L., Lamba, J.J.S., Burgin, T.P., Whitesides, G.M., Allara, D.L., Parikh, A.N., and Atre, S. (1995). Self-assembled monolayers and multilayers of conjugated thiols, .alpha.,.omega.-Dithiols, and thioacetyl-containing adsorbates. Understanding attachments between potential molecular wires and gold surfaces. J. Am. Chem. Soc. *117*, 9529–9534.

39. Lee, J., and Lee, M. (2016). Laser-induced conversion of Au powders to highly stable nanoparticles with a narrow size distribution. J. Phys. Chem. C *120*, 13256–13262.

40. Fong, Y.Y., Gascooke, J.R., Visser, B.R., Harris, H.H., Cowie, B.C., Thomsen, L., Metha, G.F., and Buntine, M.A. (2013). Influence of cationic surfactants on the formation and surface oxidation states of gold nanoparticles produced via laser ablation. Langmuir *29*, 12452–12462.

41. Berendsen, H.J.C., van der Spoel, D., and van Drunen, R. (1995). GROMACS: a message-passing parallel molecular dynamics implementation. Comput. Phys. Commun. *91*, 43–56.

42. Pronk, S., Páll, S., Schulz, R., Larsson, P., Bjelkmar, P., Apostolov, R., Shirts, M.R., Smith, J.C., Kasson, P.M., van der Spoel, D., et al. (2013). GROMACS 4.5: a high-throughput and highly parallel open source molecular simulation toolkit. Bioinformatics *29*, 845–854.

43. Ramezani, F., Habibi, M., Rafii-Tabar, H., and Amanlou, M. (2015). Effect of peptide length on the conjugation to the gold nanoparticle surface: a molecular dynamic study. Daru *23*, 9.

44. Riccardo, F., and Pietro, T. (2009). Mass Spectrometry in Grape and Wine Chemistry (Wiley).

45. Yang, C., Uertz, J., Yohan, D., and Chithrani, B.D. (2014). Peptide modified gold nanoparticles for improved cellular uptake, nuclear transport, and intracellular retention. Nanoscale *6*, 12026–12033.

46. Flora, S.J.S., and Pachauri, V. (2010). Chelation in metal intoxication. Int. J. Environ. Res. Public Health *7*, 2745–2788.

47. Gupta, A., Chaudhary, A., Mehta, P., Dwivedi, C., Khan, S., Verma, N.C., and Nandi, C.K. (2015). Nitrogen-doped, thiol-functionalized carbon dots for ultrasensitive Hg(II) detection. Chem. Commun. (Camb.) *51*, 10750–10753.

48. Bei, F., Hou, X., Chang, S.L.Y., Simon, G.P., and Li, D. (2011). Interfacing colloidal graphene oxide sheets with gold nanoparticles. Chemistry *17*, 5958–5964.

49. Liu, Y., Shipton, M.K., Ryan, J., Kaufman, E.D., Franzen, S., and Feldheim, D.L. (2007). Synthesis, stability, and cellular internalization of gold nanoparticles containing mixed peptide-poly(ethylene glycol) monolayers. Anal. Chem. *79*, 2221–2229.

50. Ostolska, I., and Wiśniewska, M. (2014). Application of the zeta potential measurements to explanation of colloidal Cr2O3 stability mechanism in the presence of the ionic polyamino acids. Colloid Polym. Sci. *292*, 2453–2464.

51. Ard, P.G., Chatterjee, C., Kunjibettu, S., Adside, L.R., Gralinski, L.E., and McMahon, S.B. (2002). Transcriptional regulation of the mdm2 oncogene by p53 requires TRRAP acetyltransferase complexes. Mol. Cell. Biol. *22*, 5650–5661.

52. Rozan, L.M., and El-Deiry, W.S. (2007). p53 downstream target genes and tumor suppression: a classical view in evolution. Cell Death Differ. *14*, 3–9.

53. Nakano, K., and Vousden, K.H. (2001). PUMA, a novel proapoptotic gene, is induced by p53. Mol. Cell *7*, 683–694.

54. Beckerman, R., and Prives, C. (2010). Transcriptional regulation by p53. Cold Spring Harb. Perspect. Biol. *2*, a000935.

55. Willard, M.D., Schall, W.D., Nachreiner, R.F., and Shelton, D.G. (1982). Hypoadrenocorticism following therapy with o,p-DDD for hyperadrenocorticism in four dogs. J. Am. Vet. Med. Assoc. *180*, 638–641.

56. Sinha, S., Malonia, S.K., Mittal, S.P., Singh, K., Kadreppa, S., Kamat, R., Mukhopadhyaya, R., Pal, J.K., and Chattopadhyay, S. (2010). Coordinated regulation of p53 apoptotic targets BAX and PUMA by SMAR1 through an identical MAR element. EMBO J. *29*, 830–842.

57. Dornan, D., Wertz, I., Shimizu, H., Arnott, D., Frantz, G.D., Dowd, P., O'Rourke, K., Koeppen, H., and Dixit, V.M. (2004). The ubiquitin ligase COP1 is a critical negative regulator of p53. Nature *429*, 86–92.

58. Leng, R.P., Lin, Y., Ma, W., Wu, H., Lemmers, B., Chung, S., Parant, J.M., Lozano, G., Hakem, R., and Benchimol, S. (2003). Pirh2, a p53-induced ubiquitin-protein ligase, promotes p53 degradation. Cell *112*, 779–791.

59. Ghosh, P., Yang, X., Arvizo, R., Zhu, Z.J., Agasti, S.S., Mo, Z., and Rotello, V.M. (2010). Intracellular delivery of a membrane-impermeable enzyme in active form using functionalized gold nanoparticles. J. Am. Chem. Soc. *132*, 2642–2645.

60. Maus, L., Dick, O., Bading, H., Spatz, J.P., and Fiammengo, R. (2010). Conjugation of peptides to the passivation shell of gold nanoparticles for targeting of cell-surface receptors. ACS Nano *4*, 6617–6628.

61. Balaji, S., Mukunthan, K.S., and Kannan, N. (2014). Biol.-nanomaterials: structure and assembly. Rev. Adv. Sci. Eng. *3*, 250–260.

62. Paciotti, G.F., Myer, L., Weinreich, D., Goia, D., Pavel, N., McLaughlin, R.E., and Tamarkin, L. (2004). Colloidal gold: a novel nanoparticle vector for tumor directed drug delivery. Drug Deliv. *11*, 169–183.

63. Laurie, N.A., Donovan, S.L., Shih, C.S., Zhang, J., Mills, N., Fuller, C., Teunisse, A., Lam, S., Ramos, Y., Mohan, A., et al. (2006). Inactivation of the p53 pathway in retinoblastoma. Nature *444*, 61–66.

64. Kalmodia, S., Parameswaran, S., Yang, W., Barrow, C.J., and Krishnakumar, S. (2015). Attenuated total reflectance Fourier transform infrared spectroscopy: an analytical technique to understand therapeutic responses at the molecular level. Sci. Rep. *5*, 16649.

65. Du, W., Wu, J., Walsh, E.M., Zhang, Y., Chen, C.Y., and Xiao, Z.X. (2009). Nutlin-3 affects expression and function of retinoblastoma protein: role of retinoblastoma protein in cellular response to nutlin-3. J. Biol. Chem. *284*, 26315–26321.

66. Andrysik, Z., Kim, J., Tan, A.C., and Espinosa, J.M. (2013). A genetic screen identifies TCF3/E2A and TRIAP1 as pathway-specific regulators of the cellular response to p53 activation. Cell Rep. *3*, 1346–1354.